Discretization Mesh Design for a Magnetic Bearing in the 3D Field Analysis

Zimon Jan[1,a], Tomczuk Bronislaw[1,b], Wajnert Dawid[1,c]
[1]Opole University of Technology, Department of Industrial Electrical Engineering, Poland
[a]j.zimon@po.opole.pl, [b]b.tomczuk@po.opole.pl, [c]dawid.wajnert@op.pl

Abstract: In this paper, nonsymmetrical 12-pole (AMB12) magnetic bearings are analyzed. 3D Finite Element Method (FEM) was used for the magnetic field computations and nonlinear boundary problem was investigated. Discretization process is described for the AMB modeling, [5]. Research applies adaptation meshing method with the aid of high-order finite elements.

Keywords: Magnetic Bearing, 3D Field Analysis, Discretization Mesh

Introduction

Finite element analysis is used by most designers of electric machines to calculate integral parameters of the magnetic field and for optimization of the magnetic circuit. Mesh density has a critical influence on the solution of the magnetic field in nearly all cases of finite-element analysis. Modeling errors which are involved in the discretization process are often called approximation errors. These errors arise as a consequence of shape functions during modeling of physical problems. They should be kept as low as possible in every finite-element analysis. In order to get results that are close to exact solution, regions that are considered with special attention are the ones in which the physical properties are non-linear. For example, the edges of iron parts have to be discreted very carefully. The interface boundary equations and interior points of the nonlinear material are prescribed before mesh generation with fine elements. At the refine discretization level, new points are inserted into the domain of support of each vertex of error elements. Then the shape of elements in these regions and their neighbors are controlled using Voronoi schema.
In this paper, the influence of finite element discretization on the force and magnetic flux density distribution for the 12-poles magnetic bearings (AMB12) is presented. The integral parameters, e.g. magnetic force and the coil inductances have been also calculated.

Problem statement

FEM method is usually used for solving partial differential equations. Mesh generation technique based upon the concept of the Delaunay partition offers numerous advantages. One of the elements formed from the new triangles and their neighbors can be constructed with the aid of Delaunay's algorithm. The vertices of the new triangle defines the circumference. One of the properties of a Delaunay triangulation is that the circumference of a Delaunay triangle does not contain another Delaunay vertex in its interior. Hence, in the event that the fourth point of the quadrilateral is located within the circle which diagonal must be swapped. Otherwise, no change in the data occurs. In the event that the quadrilateral diagonal is swapped, it is necessary to check the new triangles again for additional swaps. This procedure recurs until no more swaps are necessary. Mostly, the best results in constructing the Delaunay triangulation are when we triangulate the entire objects with its four corner vertices. For each of calculation subregions, the Delaunay triangulations have to be generated separately for example, the ferromagnetic parts described by own

magnetization should be discreted especially.. In most cases they have a non-linear magnetization curve [1].

The energy W and coenergy W' densities of the calculated system can be expressed as:

$$w = \int_0^{B_p} HdB \tag{1}$$

$$w' = \int_0^{H_p} BdH \tag{2}$$

In the vertices of the generated elements of the mesh, the unknown values of the magnetic scalar potential Ω and the vector electric potential $\vec{T}$ were assumed. Sometimes, there are subregions which are moving under operation. For example, in the magnetic bearings, the rotor is moving. Its subregions could be described with the equation $\vec{H} = -\nabla\Omega(x, y, z)$. The magnetic scalar potential $\Omega(x, y, z)$ is approximated by the combination of the linear shape function

$$\Omega(x, y, z) = \sum_i a_i(x, y, z)\Omega_i \tag{3}$$

The energy in the computational region can be calculated from:

$$W(\Omega(x, y, z)) = \int_V \left(\int_0^B HdB \right) dV + \int_\Gamma \left(H_n \, \Omega \, d\Gamma \right) \tag{4}$$

while the functional of the coenergy could be expressed by

$$W'(\Omega(x, y, z)) = \int_V \left(\int_0^H BdH \right) dV + \int_\Gamma \left(B_n \, \Omega \, d\Gamma \right). \tag{5}$$

After solving the problem for the partial differential equation, we can obtain many magnetic field integral parameters: forces, inductances and stiffness coefficients [3]. the virtual work method is very efficient for the magnetic force calculation. It requires coenergy solutions for two different rotor positions $F = -\frac{\Delta W'}{\Delta s} = \frac{W_2' - W_1'}{s_2 - s_1}$ (6)

In some cases, we can to modify this method with using the equations (4) and (5). The virtual deformation of the discretization mesh elements can be employed in calculations in which the step by step virtual work method is used [2]. This deformation could be achieved as a result of virtual infinitesimal displacement of some nodes. Each of the virtual nodes neighbored to the moving part is described by local co-ordinates (*u, v, w*), which are transformed to global ones (*x, y, z*). In this case, the approximate shapes function in this subregion for all of finite element volumes ($\sum_e$) of the rotor subregion is described as

$$\iiint_{V_w} q(x, y, z)dxdydz = \sum_e \iiint_{V_e} q(x, y, z)dxdydz = \sum_e \iiint_{V_e^*} q\big(x(u, v, w), y(u, v, w), z(u, v, w)\big) \cdot |G| \, dudvdw \tag{7}$$

where: $q(x, y, z)$ denotes any function;

V_e, V_e^* are respectively the volumes of the real and virtual elements

$|G|$ is the determinant of the Jacobean transformation

After the coenergy differentiation (Eq.5), we obtain the force

$$F_s = \frac{\partial}{\partial s}\left(\int_V \left(\int_0^H BdH\right) dV\right) + \frac{\partial}{\partial s}\left(\int_\Gamma \left(B_n \Omega d\Gamma\right)\right) \tag{8}$$

For calculation of the equation (8), some assumptions have to be made. The first one, is that the virtual displacement doesn't affect finite element displacement in the calculated region and into the subregion boundaries. The magnetostriction of the magnetic materials has to be neglected, also. Thus, the magnetic force can be calculated from

$$F_s = \frac{\partial}{\partial s}\sum_e \int_{V_e}\int_0^H BdH\, dV_e = \frac{\partial}{\partial s}\sum_e \int_{V_e^*}\left(\int_0^H BdH \cdot |G|\right) dV_e^* = \sum_e \int_{V_e^*}\left(\frac{\partial}{\partial s}\int_0^H BdH \cdot |G| + \int_0^H BdH \cdot \frac{\partial}{\partial s}|G|\right) dV_e^* \tag{9}$$

After some mathematical transformations, the one-step virtual work method for the magnetic force calculation can be expressed

$$F_s = \sum_e \int_{V_e^*}\left(-B^T G^{-1}\frac{\partial G}{\partial s}\cdot H + \int_0^H BdH \cdot |G|^{-1} \cdot \frac{\partial}{\partial s}|G|\right) dV_e^* \tag{10}$$

The mathematical review shows the influence of discretization mesh quality on the magnetic force results.

Description of the magnetic bearing

In nonsymmetrical AMB12, the excitation winding consists of 12 symmetric coils, each with *N*=40 turns, [2]. The wounded excitation coils creates six horseshoe electromagnets, which creates four sections. They are situated in a way that makes it possible to excite four independent fluxes. Each of them crosses two stator poles. In order to determine the accuracy of the results from the finite element analysis four different meshes has been used for discretization of a quarter of 12-poles active magnetic bearing. Its configuration with coils is presented in Fig.1. The most important AMB dimensions are given in Table 1.

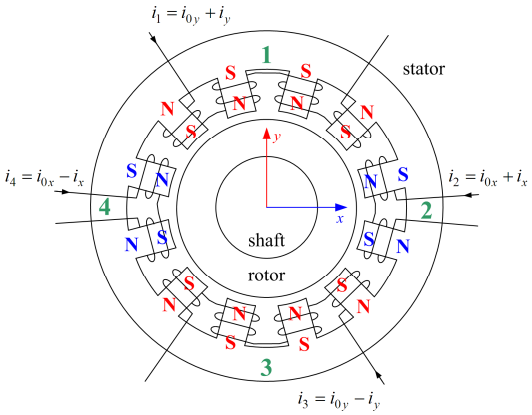

Fig. 1 General configuration of 12-poles AMB

Table 1. Main AMB dimensions

Parameters	**Value** [mm]
Stator outer diameter	100
air gap	1
Rotor diameter	56
Stator length	56
Rotor length	80

We calculated 4 variants of generation meshes for the 12-poles AMB:

a) Mesh 1 consists of 27,385 elements. It is default mesh nets generated automatically by the Delanuay method using the defined boundary between the regions only, Fig. 2a. The number of nonzero stiffness matrix elements for FEM was 37,275. The convergence time after eight Newton-Raphson iterations was 66 seconds of CPU. The mesh generation time was 54 s.

b) Mesh 2 is discreted with 270,955 elements. This mesh variant contains of the circumcircuit definition for the stator and rotor regions. The maximum edge length of the tetrahedral element is defined by 10mm. The aspect ratio for the edge length is 3. The boundary problem characterizes with 375,311 variables and convergence time 510 [s] for tree Newton-Raphson iterations. The mesh was generated in 265 seconds.
c) Mesh 3 consists of 471,443 elements. Additionally, the mesh 2 was changed for air gap subregion. The maximum edge length is 1mm. Thus, in the airgap subregion 2-elements distance between the stator and rotor was achieved. After mesh generation (about 519 seconds), the field problem was solved also with tree iterations in time 703 seconds.
d) Mesh 4 is divided into 810,330 elements. We upgraded the mesh 3 with the maximum edge length 0.7 mm for the airgap subregion, (Fig. 2b). The mesh generation time was 1,060 seconds of the processor time. The solution of the equation system with 1,100,046 variables, after tree Newton-Raphson iteration was achieved after 1,409 seconds of CPU time.

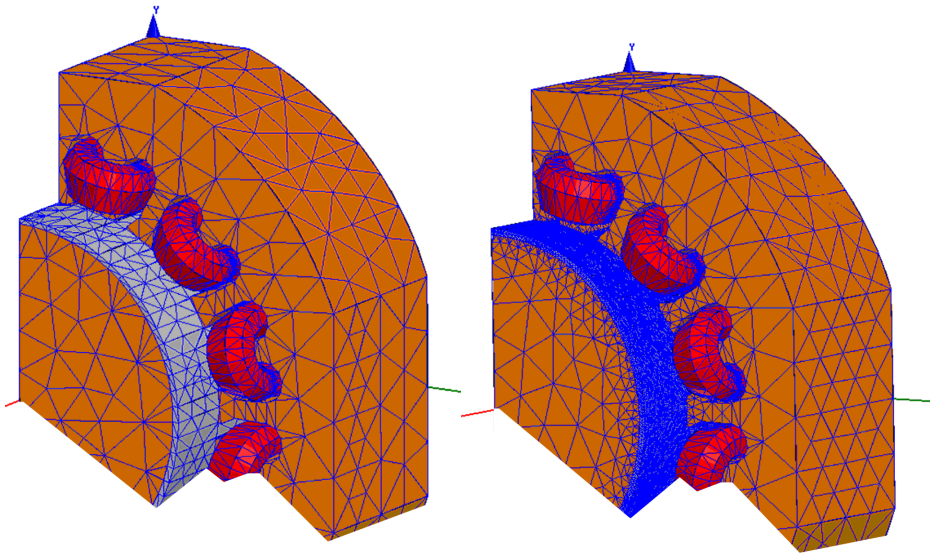

Fig 2. Finite element mesh discretization: a) Mesh 1, b) Mesh 4

The boundary problems were solved on the INTEL XEON E5404 Workstation with 32GB of RAM, and 1TB of RAID(0) hard drive matrix. Mesh generation and convergence times vs. number of elements is shown in Fig. 3.

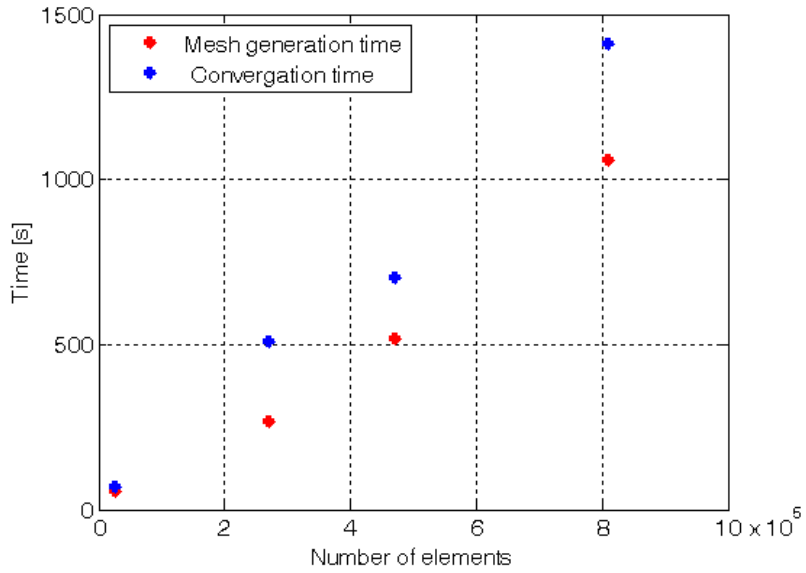

Fig 3. Mesh generation and convergence times vs. number of elements

It can be observed that the time discretization and the solution time increase faster for a large number of elements (Mesh 4).

Field calculation results and the test result

Measurement accuracy of the flux density components is concerned with the precision of the hall sensor positioning. We used the measurement system with 8 hall sensors. Linear characteristic of each sensor output voltage has been included. The 10-bit resolution of the A/C converter have been taken into consideration for the flux density measurement in two ranges of $\pm 40\text{mT}$ and $\pm 100\text{mT}$. The relative error of 2% was determined for the tests.

The measurement line LN1 has been chosen in the air gap between stator and rotor (Fig.5). The measured components of flux density include the ones that are longitudinal B_z and perpendicular B_r, to the main axis of symmetry (Fig.6).

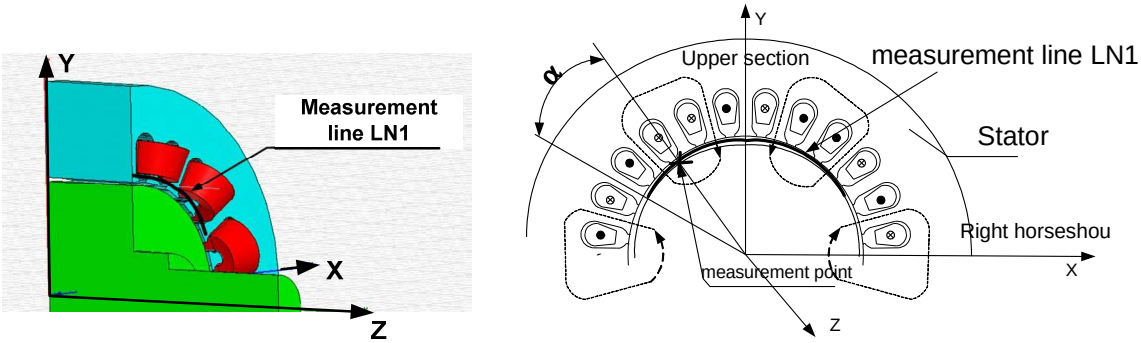

Fig. 5. Line with the points in which the B components were tested.

After solving the boundary problem, we can calculate the flux density values. It is performed for several positions of the AMB rotor. In Fig. 6 we compare the computational results with the measured ones.

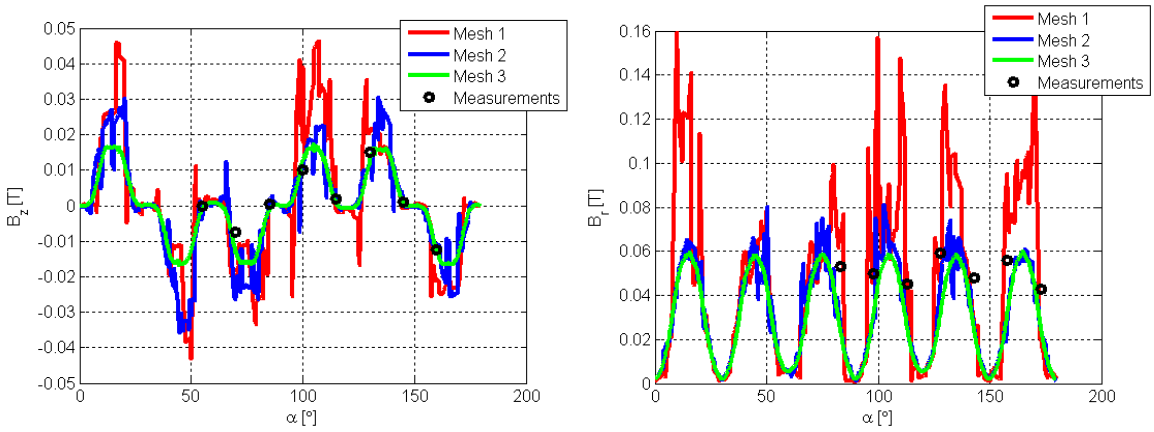

Fig. 6. Magnetic flux density distribution verso the angle degrees.
a) B_z component, b) B_r component

The degrees in Fig.6 determine the angles between the radius through the points at which the B components have been measured and x axis. The figure presents magnetic flux distributions for the three discretization meshes are drawn. One ought to add that the mesh 1 and mesh 2 are not optimal for the field calculations. We can see additional peaks in B_z and B_r diagrams caused by the calculation errors. The errors are more than 100% of the real value. The computational results for the discretization according the mesh 3 are conformable with the real changes of flux density. The calculation values very fine mesh 4 are not presented in the figures. They are very close to the results obtained with the mesh 3. Thus mesh 3 is the optimal discretization mesh for the field analysis of the presented object.

After the field computation we are able to compute the magnetic force on the AMB rotor. The resulting force excited by the coils that operates along Y axis is presented in Fig. 7.

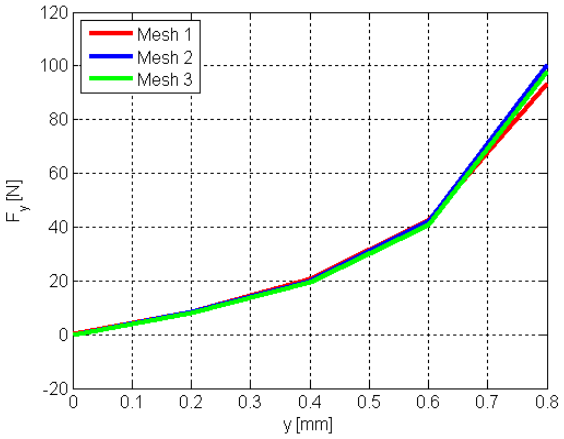

Fig 7. Magnetic force vs. rotor displacement

The magnetic force is the integral parameter of the field. Thus it depends on the discretization of the calculated area. However, the integral parameters do not depend on the discretization as strongly as flux density values. Fig. 7 shows a comparison of the force values calculated by the energy method with meshes 1, 2 and 3. It is visible that the results obtained from the meshes are close. Only the results obtained with using the mesh 1 are not sufficiently accurate. The coarse discretization can be used for the prediction of the force.

Conclusions

The effect of mesh discretization on the magnetic flux density and force calculation for the AMB have been discussed. The dependence between magnetic flux density distribution and mesh density for discretization of the analysed area provides the appropriate discretization with the mesh density for a finite element model. The prediction of magnetic force in AMB and in other bearings may be convenient to incorporate the adaptive meshing algorithm. The finest mesh ensures the best accuracy of flux density and magnetic force calculations in a magnetic device. However, it results in the extended time needed for the computation. Moreover, there is a need of an operating memory with high capacity. Due to addition of the field values errors at the individual points of the analysed area the field integral parameters can be determined for the more coarse mesh.

References

[1] Tomczuk B., Zimon J., Field determination and calculation of stiffness parameters in an active magnetic bearing (AMB), Solid State Phenomena Vols. 147-149, 2009, pp. 125-130
[2] Zimon J., Field Analysis and Parameters Computation in the Active Magnetic Bearings, Doctoral Thesis, Opole, 08.01.2009
[3] B. Tomczuk, J. Zimon, A. Waindok, Effects of the Core Materials on Magnetic Bearing Parameters", Compumag'09, PA1.16, 22-27.11.2009, Florianopolis, Brasil, pp. 39-40
[4] Schweitzer G., Traxler A., Bleurer H., Magnetlager, Springer Verlag, Heidelberg, 1993.
[5] Zhou, P., Fu, W.N., Lin, D., Stanton, S., Cendes, Z.J., Numerical modeling of magnetic devices, IEEE Trans. on Mag, Vol. 40/4, 2004, pp. 1803-1809
[6] J. F. Lee, D. K. Sun and Z. J. Cendes, "Tangential Victor Finite Elements for Electromagnetic Field Computation", CEFC, Toronto, Oct. 1990, Vol. 27/5, pp. 3958-3966